The Journal of Neuroscience, April 15, 1999, 19(8):2906–2918

Functional Analysis of a Mouse Brain Elk-Type K^+ Channel

Matthew C. Trudeau,[1] Steven A. Titus,[2] Janet L. Branchaw,[1] Barry Ganetzky,[2] and Gail A. Robertson[1]

[1]Department of Physiology, University of Wisconsin-Madison Medical School, and [2]Laboratory of Genetics, University of Wisconsin, Madison, Wisconsin 53706

Members of the Ether à go-go (Eag) K^+ channel subfamilies Eag, Erg, and Elk are widely expressed in the nervous system, but their neural functions *in vivo* remain largely unknown. The biophysical properties of channels from the Eag and Erg subfamilies have been described, and based on their characteristic features and expression patterns, Erg channels have been associated with native currents in the heart. Little is known about the properties of channels from the Elk subfamily. We have identified a mouse gene, *Melk2*, that encodes a predicted polypeptide with 48% amino acid identity to *Drosophila* Elk but only 40 and 36% identity with mouse Erg (Merg) and Eag (Meag), respectively. *Melk2* RNA appears to be expressed at high levels only in brain tissue. Functional expression of *Melk2* in *Xenopus* oocytes reveals large, transient peaks of current at the onset of depolarization. Like Meag currents, Melk2 currents activate relatively quickly, but they lack the nonsuperimposable Cole–Moore shift characteristic of the Eag subfamily. Melk2 currents are insensitive to E-4031, a class III antiarrhythmic compound that blocks the Human Ether-à-go-go-Related Gene (HERG) channel and its counterpart in native tissues, I_{Kr}. Melk2 channels exhibit inward rectification because of a fast C-type inactivation mechanism, but the slower rate of inactivation and the faster rate of activation results in less inward rectification than that observed in HERG channels. This characterization of Melk currents should aid in identification of native counterparts to the Elk subfamily of channels in the nervous system.

Key words: Melk2; Elk; Eag; brain; channel; C-type inactivation

Members of the Ether-à-go-go (Eag) family of K^+ channels are expressed across a broad range of species and tissues where they serve diverse physiological roles. The observation that mutations in the *Drosophila* gene *eag* cause spontaneous action potentials in motor neurons and enhanced transmitter release at the *Drosophila* neuromuscular junction (Ganetzky and Wu, 1983; Wu et al., 1983) was the first indication that these genes regulate membrane excitability. The subsequent cloning of *eag* (Drysdale et al., 1991; Warmke et al., 1991) led to the identification of many related genes including the *Human Ether-à-go-go-Related Gene* (*HERG*; Warmke and Ganetzky, 1994), which is critical for maintaining the normal rhythmic activity of the human heart (Curran et al., 1995).

Several members of the Eag and Erg subfamilies have been expressed in heterologous systems with the aim of using the biophysical and pharmacological properties revealed by such studies to identify their corresponding currents in native tissues. Within the Eag subfamily, all mammalian representatives identified to date have properties typical of delayed rectifiers with no measurable inactivation (Ludwig et al., 1994; Robertson et al., 1996; Frings et al., 1998); only *Drosophila* Eag channels exhibit partial inactivation (Robertson et al., 1996). A shared characteristic of members of the Eag subfamily is a nonsuperimposable Cole–Moore shift (Ludwig et al., 1994; Robertson et al., 1996), in which the time course of activation becomes slower and more sigmoidal as the prepulse or holding potential is made more negative and, as a consequence, the currents do not superimpose when aligned by shifting along the time axis (Cole and Moore, 1960; Young and Moore, 1981).

In contrast to Eag channels, all Erg channels studied to date exhibit significant inactivation. HERG channels open and then rapidly enter a highly stable inactivated state during depolarization, effectively suppressing outward current at positive voltages (Sanguinetti et al., 1995; Trudeau et al., 1995) (cf. Shibasaki 1987). The predominant current thus occurs during repolarization as channels recover from inactivation and slowly deactivate (Zhou et al., 1998) (cf. Zeng et al., 1995). These unusual gating properties together with a sensitivity to the pharmacological agent E-4031 suggested that HERG subunits underlie cardiac I_{Kr} (like that described in native tissues by Sanguinetti and Jurkewicz, 1990) and led to the conclusion that mutations in *HERG* cause long QT syndrome by disrupting this repolarizing current (Sanguinetti et al., 1995; Trudeau et al., 1995). As such, HERG is the only member of the Eag family with a clearly defined native counterpart and physiological role.

We have identified a member of the Elk subfamily from mouse (Melk2) which, based on sequence analysis, defines a separate subclass within the Elk subfamily distinct from a rat channel first identified (Relk1; S. Titus and B. Ganetzky, unpublished data) (Shi et al., 1998). We find that *Melk2* mRNA is expressed at high levels only in the brain. In contrast to Eag or Erg currents, Melk2 currents expressed in *Xenopus* oocytes exhibit a large, transient outward component during depolarization. If presented with a

Received Oct. 2, 1998; revised Jan. 29, 1999; accepted Feb. 1, 1999.

This work was supported by National Institutes of Health Grant HL55973 and a National Science Foundation Career Award to G.A.R., a predoctoral fellowship from the American Heart Association-Wisconsin to M.C.T., and National Institutes of Health Grant NS15390 to B.G. The Melk2 sequence has been deposited in GenBank with accession number AF109143. We thank Cena Meyers for technical assistance, Elon Roti Roti and Nathan Penn for frog surgery and oocyte preparation, and Eisai (Tokodai, Japan) for providing E-4031. Thanks to Jinling Wang and Dr. Ed Chapman for helpful discussions and Jinling Wang for critically reading this manuscript.

Correspondence should be addressed to Dr. Gail Robertson, Department of Physiology, University of Wisconsin-Madison Medical School, 1300 University Avenue, Madison, WI 53706.

Dr. Trudeau's present address: Department of Physiology and Biophysics, Howard Hughes Medical Institute, University of Washington, Box 357370, Seattle, WA 98195.

Figure 1. Amino acid sequence alignment of Melk2. Sequence comparisons of Melk2, *Drosophila* Elk, Meag, and HERG were made using Lasergene's Clustal method (DNAstar). Identical amino acids are indicated by the *black shading*, and gaps in the sequence are indicated by *dashes*. Amino acids are *numbered* on the *right*. The membrane-spanning regions (*S1–S6*), the pore domain of the hydrophobic core and the region of homology with a cyclic nucleotide binding domain (*cNBD*) are indicated by *lines* above the sequence. *Asterisks* indicate the residues mutated for experiments described in Figure 10.

subsequent repolarizing ramp, a second component of outward current is evoked as channels recover from inactivation and revisit the open state before closing. These properties suggest that Melk2 channels may participate in action potential repolarization as well as regulation of burst properties. A detailed characterization is presented here to facilitate the identification of Melk2 currents in native tissues.

MATERIALS AND METHODS

Molecular biology. A computer-based search of a mouse dBEST database identified a partially sequenced (190 bp) mouse brain cDNA encoding a polypeptide segment that had significant similarity with the corresponding region of the *Drosophila* Elk polypeptide. This cDNA (IMAGE consortium number 319419) was obtained and sequenced on both strands using automated fluorescent sequencing (model 377; Applied Biosystems, Foster City, CA). Sequence analysis indicated that this cDNA encodes the complete open reading frame of a member of the Elk subfamily of potassium channels, which we named *Melk2*. Sequence alignments were generated and analyzed using Lasergene software programs (DNAstar, Madison, WI).

For oocyte expression studies, the *Melk2* cDNA was subcloned into a derivative of the pGEMHE expression vector (Liman et al., 1992) and linearized at the *Not*I site for cRNA transcription. The *HERG* and *Meag* constructs used here were previously described (Trudeau et al., 1995, 1996; Robertson et al., 1996). Point mutations in *Melk2* were generated with a PCR-based approach using mutagenic primers (Higuchi et al., 1990). All sequences generated by PCR were confirmed by sequencing on both strands as described above.

The distribution of the *Melk2* transcript was assessed using a mouse multiple tissue Northern blot (Clontech, Palo Alto, CA) probed with a ^{32}P-labeled fragment corresponding to the 3′ end of *Melk2* from bp 2410–2880. High-stringency conditions were used with ExpressHyb solution (Clontech). Bands were visualized after a 3 d exposure to Biomax MS film at −70°C.

Oocyte handling and RNA preparation. Procedures used for oocyte preparation were the same as those detailed previously (Herzberg et al., 1998). Oocytes were surgically removed from anesthetized female frogs (*Xenopus laevis*, Nasco) and defolliculated by treatment with 1 mg/ml collagenase B (Boehringer Mannheim, Indianapolis, IN), followed by an osmotic shock procedure (Pajor and Wright, 1992). cRNAs were transcribed from the T7 promoter of DNA templates using the mESSAGE mACHINE kit (Ambion, Austin, TX) and diluted in sterile water to yield ~20 ng of cRNA per oocyte in an injection volume of 37 nl. Oocytes were injected using a Drummond microinjector, after which they were stored for 1–7 d at 18°C in standard ND-96 solution (in mM: 96 NaCl, 2 KCl, 1 $MgCl_2$, 1.8 $CaCl_2$, and 5 HEPES, pH 7.4) supplemented with 10 μg/ml gentamycin sulfate.

Electrophysiological measurements and analysis. Currents were recorded with the two-electrode voltage-clamp technique (OC-726C; Warner, Hamden, CT) after 1–7 d incubation. All experiments were conducted at room temperature (21–23°C). Data were sampled at 1 kHz. Electrode resistances were 0.5–1 MΩ when filled with 2 M KCl. The bath solution contained (in mM): 95 NaCl, 5 KCl, 1 $MgCl_2$, 0.3 $CaCl_2$, and 5 HEPES, adjusted to pH 7.4 with NaOH, unless otherwise noted. Data acquisition and analysis were performed with pClamp 6.0 software (Axon Instruments, Foster City, CA). Curve fitting in Clampfit was performed using the Chebyshev method. Additional analysis and Boltzmann curve fits were performed with Origin 4.0 software (Microcal, Amherst, MA). In some cases, small corrections for leak were made using an off-line linear leak subtraction protocol in Clampfit (based on current evoked at voltage steps to −100 mV), but correction was often not necessary because of negligible leak (<1% of total conductance). If leak exceeded 10% of total conductance, the data were discarded. Sample numbers (n) refer to the number of individual oocytes recorded.

The permeability ratio for Na^+ and K^+ was determined from a simplified form of the Goldman–Hodgkin–Katz equation, where the reversal potential $E_{rev} = 58 \log \{[P_{Na}(Na)_{out} + P_K(K)_{out}]/[P_{Na}(Na)_{in} + P_K(K)_{in}]\}$, and we have assumed no permeability to Cl^- ions. E_{rev} for Melk2 was determined from the experiments in Figure 5*A*; K_{out} and Na_{out} were 5 and 95 mM, respectively. Values for K_{in} and Na_{in} are 92.5 and 6.2 mM, respectively, as reported by Barish (1983).

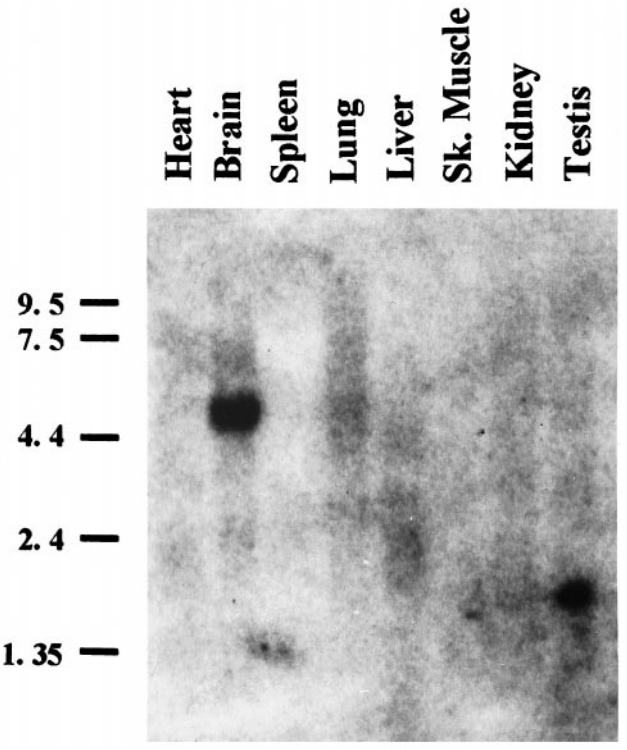

Figure 2. Tissue expression of Melk2. A mouse multiple tissue Northern blot (Clontech) was probed using a ^{32}P-labeled C-terminal fragment of Melk2 corresponding to bp 2410–2880 under high-stringency conditions. A single band of ~5 kb was observed specifically in brain.

RESULTS

Sequence analysis of Melk channels

A partially sequenced mouse brain cDNA encoding a polypeptide segment with strong amino acid similarity with the *Drosophila* Elk sequence was identified in a computer-based search of a mouse dBEST database. As shown by the alignment in Figure 1, the predicted polypeptide encoded by this cDNA shares significant similarity with other members of the Eag family of potassium channel polypeptides across its entire length. Because the highest degree of identity is shared with members of the Elk subfamily, the sequence was named Melk (for mouse Elk). For the core of the polypeptide, extending from the S1 domain through the region with homology to previously characterized cyclic nucleotide binding domains (cNBD-like domain), Melk exhibits 38% amino acid identity with Meag, 45% identity with HERG, 48% identity with *Drosophila* Elk, and 63% identity with a rat Elk (Relk1) gene cloned from rat sciatic nerve (Titus and Ganetzky, unpublished data) (Shi et al., 1998). Sequence comparisons among Melk, Relk and a recently identified human Elk (Helk; Titus and Ganetzky, unpublished data) indicate that there are at least two Elk subtypes in mammals. One subtype is defined by Relk1, which is ~63% identical (S1 through the cNBD-like domain) with either Melk or Helk. The mouse and human Elk sequences share 97% identity and thus appear to belong to a second subclass. Because we obtained the Relk sequence before that of Melk or Helk, we refer to the mouse polypeptide characterized here as Melk2.

A multiple tissue Northern blot probed with a fragment from the C terminus of Melk2 (bp 2410–2880) revealed a single tran-

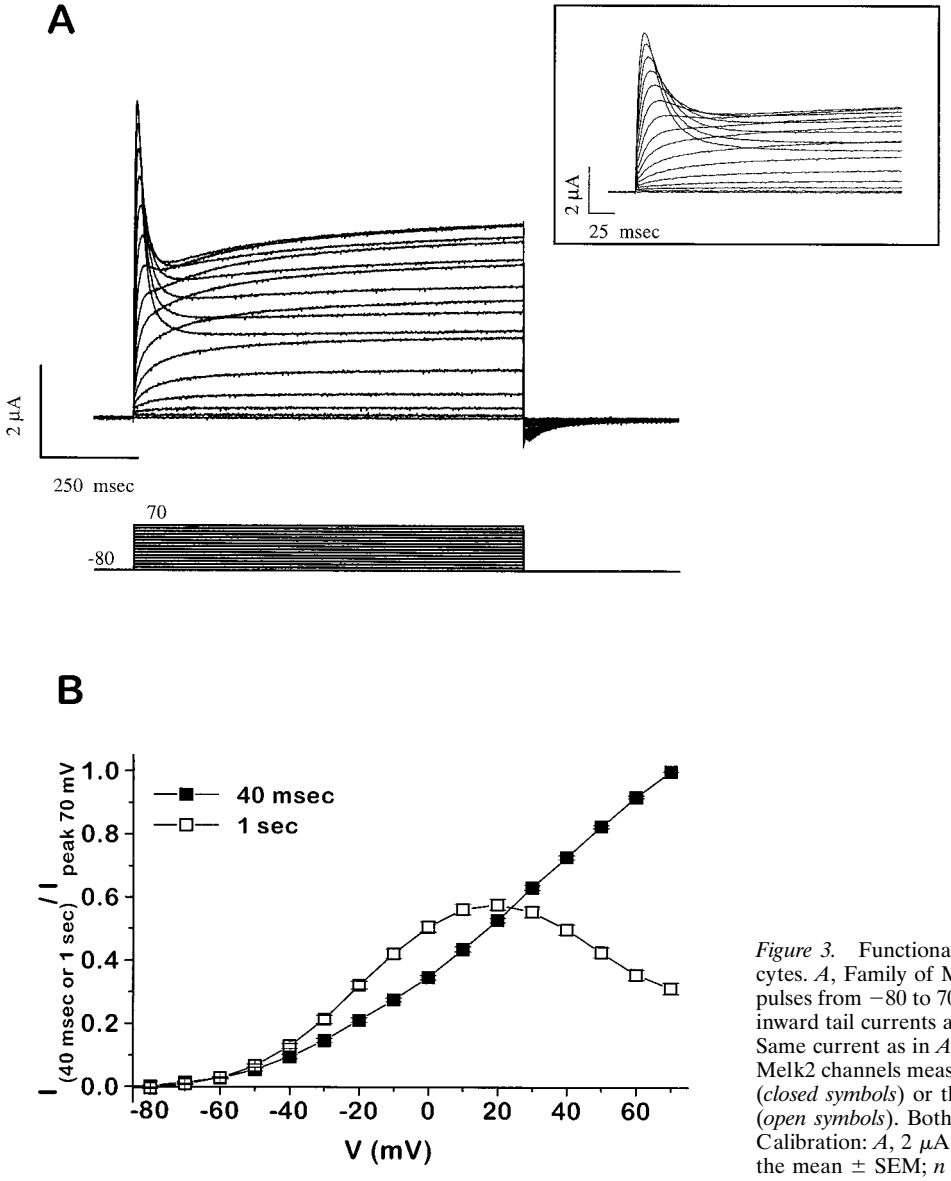

Figure 3. Functional expression of Melk2 channels in *Xenopus* oocytes. *A*, Family of Melk2 currents generated in response to voltage pulses from −80 to 70 mV from a holding potential of −80 mV. Small inward tail currents are visible after repolarization to −80 mV. *Inset*, Same current as in *A* but on a shorter time scale. *B*, *I–V* relations for Melk2 channels measured at the peak current within the first 40 msec (*closed symbols*) or the current at the end of the 1 sec voltage pulse (*open symbols*). Both are normalized to the peak current at 70 mV. Calibration: *A*, 2 μA, 250 msec; *inset*, 2 μA, 25 msec. *Points* in *B* are the mean ± SEM; $n = 5$.

script of 5 kb expressed specifically in brain (Fig. 2). A band of ~2 kb was detected in testis, but it has not yet been established whether this represents a bona fide Melk2 mRNA isoform.

Functional expression of Melk2 channels in *Xenopus* oocytes

To characterize the functional properties of Melk2 channels, we performed two-electrode voltage-clamp analysis of Melk2 currents expressed heterologously in *Xenopus* oocytes. With voltage steps up to ~0 mV the currents are sustained, with little evidence of inactivation (Fig. 3*A*). At more positive voltage steps, currents have a transient, early inactivating component (see expanded view in Fig. 3*A, inset*). The peak *I–V* relation measured within the first 40 msec is relatively linear (Fig. 3*B, filled symbols*), whereas the steady-state *I–V* relation inwardly rectifies because of inactivation at voltages positive to 20 mV, giving a region of negative slope conductance (Fig. 3*B, open symbols*).

Melk2 activation kinetics

To characterize the time course of Melk2 activation, we measured the amplitude of the tail current evoked at progressively longer times after a depolarizing pulse to obtain time-dependent increases in conductance (Fig. 4*A*, Table 1). This method, used for measuring activation in HERG channels (Trudeau et al., 1995), ensures that temporal overlap with the inactivation process does not confound measurements of activation. The macroscopic activation time course thus determined can be described by two exponentials with an early rapid component ($\tau = 3.71 \pm 0.71$ msec at 70 mV) followed by a slower component ($\tau = 36.0 \pm 3.6$ msec at 70 mV; $n = 8$). Activation kinetics are faster at more positive voltages (Fig. 4*B*, Table 1).

A defining characteristic of activation in *Drosophila* and mammalian Eag channels (Ludwig et al., 1994; Robertson et al., 1996; Terlau et al., 1996) is the presence of a Cole–Moore shift in which activation becomes slower and more sigmoidal with successively more hyperpolarizing prepulses (Young and Moore, 1981). To determine whether Melk2 channels exhibit a Cole–Moore shift, we varied the prepulse potential and measured the activation kinetics of currents evoked by a subsequent step to 70 mV using the tail current pulse protocol described above (compare Fig. 4). As shown in Figure 5*A*, Melk2 activation kinetics were not

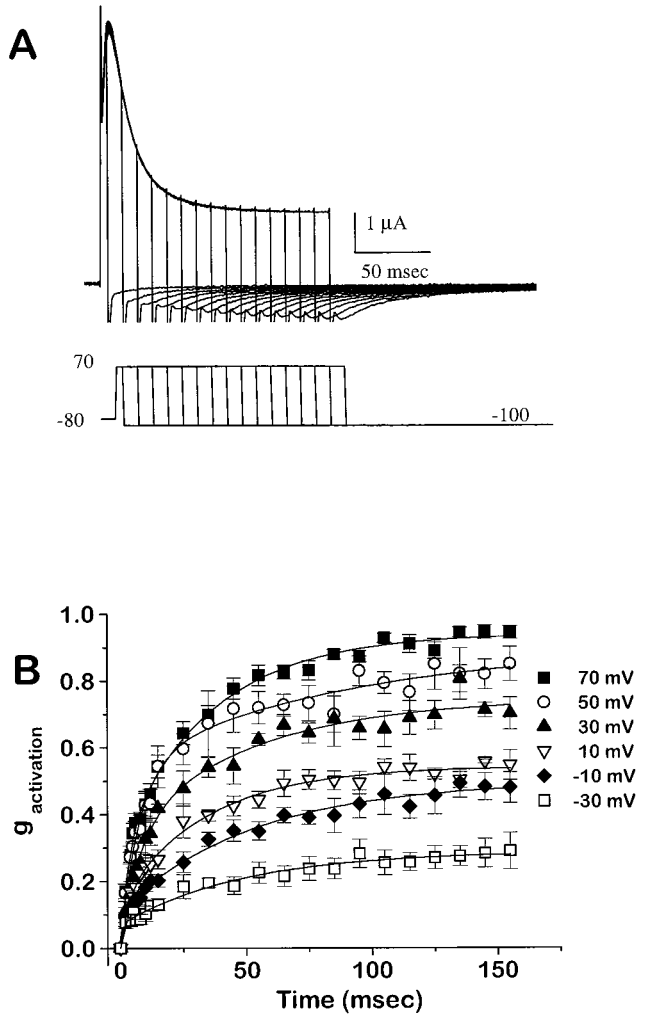

Figure 4. Activation in Melk2 channels. *A*, Melk2 activation kinetics measured with an envelope voltage paradigm in which a series of pulses to 70 mV that increase in either 2 or 10 msec durations were given from rest at −80 mV. The resulting tail current at −100 mV was fit with the sum of two exponentials ($y = A_{fast}e^{-(t/\tau fast)} + A_{slow}e^{-(t/\tau slow)}$) and extrapolated to the onset of the voltage pulse (t = 0 msec). (*B*) These values were plotted versus time and normalized to the peak tail current at 70. The same experiment in *A* was performed at other voltages, as indicated in *B*. The points in *B* represent the activation kinetics and were best fit with the sum of two exponentials [$y = 1 - (A_{fast}e^{-(t/\tau fast)} + A_{slow}e^{-(t/\tau slow)})$]; the time constants from these fits are reported in Table 1. Calibration: 1 μA, 50 msec.

measurably altered by prepulses over the range of −120 to −80 mV, in contrast to the effect of prepulse on kinetics of Meag current activation (Fig. 5*B*). Like Melk2, HERG activation kinetics are insensitive to prepulse voltage (Fig. 5*C*), suggesting that the presence of the Cole–Moore shift may distinguish channels in the Eag subfamily from those in the Elk or Erg subfamilies.

Consistent with the absence of a Cole–Moore shift is the lack of sensitivity of Melk2 activation kinetics to increases in external Mg^{2+} concentration (Fig. 5*D*). In mammalian Eag channels, elevated divalent cation concentrations cause activation to become slower and more sigmoidal in a manner reminiscent of the Cole–Moore shift caused by changes in the prepulse potential (Terlau et al., 1996). Elevation of external Mg^{2+} concentration causes a reduction of the inward Melk2 tail current, as represented by the points in Figure 5*D*, *inset*. However, when these data sets are scaled they superimpose, demonstrating that Melk2 activation kinetics are unaffected by changes in external Mg^{2+} concentration (Fig. 5*D*). Thus, Melk2 channels can be distinguished from channels in the Eag subfamily by their lack of a Cole–Moore shift and the insensitivity of their activation kinetics to external divalent cation concentration.

Table 1. Activation time constants as in Figure 4

	Activation τ (msec)	
V_m (mV)	Fast	Slow
10	11.54 ± 3.5	82.5 ± 8.5
30	7.73 ± 3.16	70.0 ± 5.5
50	5.08 ± 1.8	55.1 ± 7.3
70	3.71 ± 0.71	36.0 ± 3.6

Values are mean ± SD; $n = 8$ at 70 mV; $n = 4$ at all other voltages.

Melk2 deactivation kinetics

To measure Melk2 deactivation kinetics, the channels were first activated with a voltage step to 70 mV followed by a series of steps from 20 to −120 mV to close (deactivate) the channels (Fig. 6*A*). The deactivation time course is reflected in the decay of these currents, which is generally preceded by a faster, initial rising phase as channels recover from inactivation via the open state. The decay phase was best fit with the sum of two exponentials, with a fast deactivation component ranging from 107.7 ± 22.6 msec at −20 mV to 38.5 ± 7.0 msec at −120 mV and a slow component ranging from 380 ± 127 msec at −20 mV to 223.2 ± 57 msec at −120 mV ($n = 10$; Fig. 6*B*, Table 2). The fast component accounted for 60–80% of the fit over the range of voltages tested.

Tail currents in Figure 6*A* were also used to determine the permeability ratio for Na^+ and K^+ ions in Melk2 channels. The reversal potential determined from these experiments was −70.6 ± 0.4 mV ($n = 4$), and solving the Goldman–Hodgkin–Katz equation (see Materials and Methods) gave a permeability ratio (P_{Na}/P_K) of 0.007, indicating that Melk2 channels allow one Na^+ ion to permeate for every 150 K^+ ions.

Melk2 inactivation kinetics

Inactivation was measured using a three-pulse protocol similar to that used in the analysis of HERG channels to isolate inactivation from the temporally overlapping activation process (Schonherr et al., 1996; Smith et al., 1996; Spector et al., 1996b; Wang et al., 1996; Herzberg et al., 1998). First, channels were maximally activated by a 1 sec pulse to 70 mV and then allowed to recover from inactivation to the open state by a brief (10 msec) step to −80 mV (Fig. 7*A*). Before significant deactivation, the channels were driven from the open state back to the inactivated state by a third voltage step ranging from 70 to 20 mV. The currents evoked at this third pulse to 70 mV were twice as large as those evoked by a single step to 70 mV (peak current shown by brackets) and decayed (inactivated) approximately three times faster (see expanded time scale to the *right*). Single exponential fits to these traces had time constants ranging from 6.0 ± 0.68 msec at 70 mV to 10.8 ± 1.15 msec at 20 mV ($n = 4$; Fig. 7*B*, Table 3). The change in time constant with voltage reflects an intrinsic voltage dependence to the Melk2 inactivation process that is distinct from the voltage dependence of activation.

Like HERG channels, Melk2 channels recover from inactivation with a time course much faster than that of deactivation and

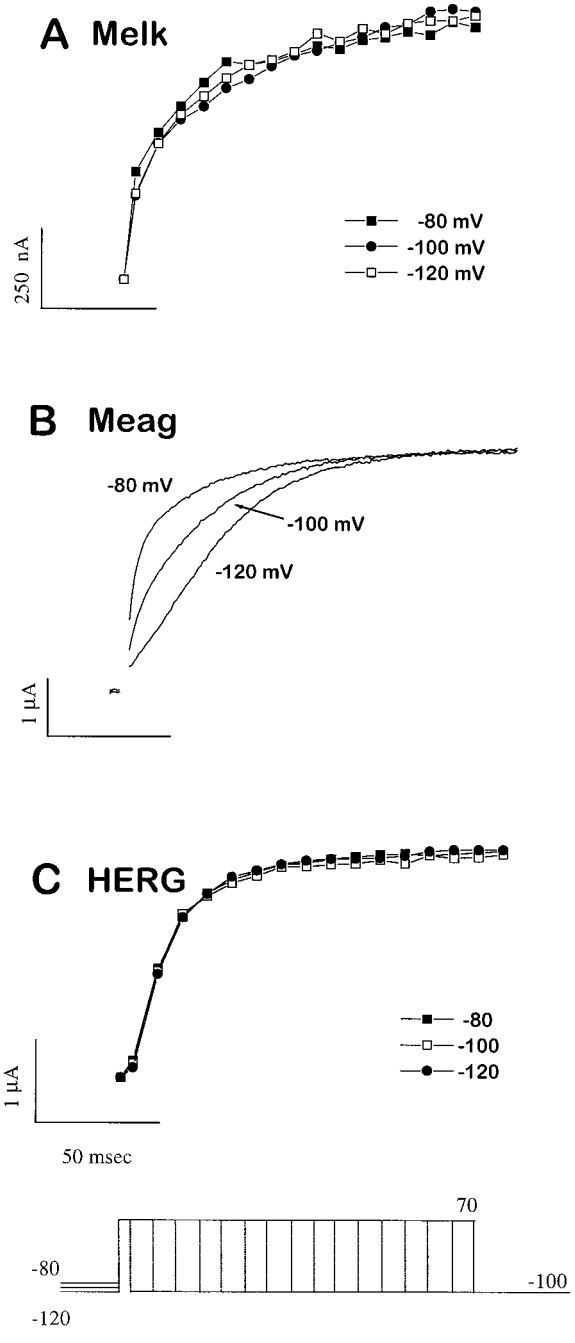

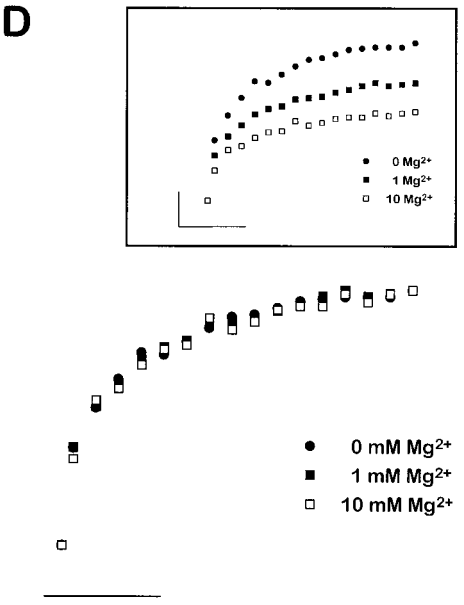

Figure 5. Effect of prepulse holding potential and external Mg^{2+} on channel activation. *A–C*, Melk2 (*A*) Meag (*B*), and HERG (*C*) activating currents at 70 mV elicited after a 500 msec prepulse holding potential of −80, −100, or −120 mV as indicated. Activation was measured for Melk2 (*A, D*) and HERG (*C*) by plotting the development of the tail current at −100 mV after pulses to 70 mV of incremental duration in steps of 10 msec, as in Figure 5. For Meag (*B*), activation is simply represented by the rise of the outward current. *D*, Melk2 activation measured in the presence of 0, 1 (normal Ringers'), or 10 mM external Mg^{2+} by the same method as in *A* and Figure 4 from a holding potential of −80 mV. Mg^{2+} reduced Melk2 tail current amplitude (*D, inset*), but scaling these currents indicates that the activation time course is not changed by Mg^{2+}. The peak tail current relative to that in the absence of Mg^{2+} was 0.80 ± 0.02 and 0.58 ± 0.01 in 1 and 10 mM Mg^{2+}, respectively (mean ± SEM; $n = 4$ for each point). Calibration: *A–D*, 50 msec; *A, D, inset*, 250 nA; *C, B*, 1 μA. The current amplitude calilbration in *A, C*, and *D* is the absolute current value for comparison with Meag. The results seen in *A–D* were also observed for three additional oocytes.

thus exhibit relatively large tail currents during repolarization. Because the recovery from inactivation is rapid, it is not always resolved in each record, but in many cases it can be seen as a rising phase of the tail current before deactivation (e.g., Fig. 6*A*). The time course of recovery could be measured by stepping from 70 mV to a range of voltages, as in Figure 6*A*; at each voltage, the resulting current was fit with a single exponential function, with time constants ranging from 16.5 ± 1.1 msec at 20 mV to 3.15 ± 0.2 msec at −80 mV ($n = 8$; Table 4). As will be discussed below, the rapid recovery from inactivation together with the rapid activation confer unique physiological properties to the Melk2 channel.

Steady-state properties of Melk2 channels

The steady-state activation properties of Melk2 channels were determined from tail current measurements. Inward tail currents were elicited by repolarizing steps to −100 mV after 3 sec test voltage steps ranging from −100 to 60 mV (Fig. 8*A*). The deactivation decay of each tail current was fit with a double exponential function and back-extrapolated to the moment of the voltage change. The resulting values were normalized to the maximum extrapolated values obtained after the step to 60 mV and plotted as relative conductances (g/g_{max}) as a function of the preceding voltage step. The values obtained using this procedure are thus an estimate of the conductances that would be measured from the instantaneous peak tail currents in the absence of inactivation, a method previously used for the analysis of HERG currents (Trudeau et al., 1995; Wang et al., 1997). The *g–V* relationship obtained in this manner has a slope factor (k) of 28.34 ± 1.55 mV per e-fold change in conductance and half-maximal voltage of activation ($V_{½}$) of −6.37 ± 1.34 mV ($n = 8$; Fig. 8*C, filled squares*).

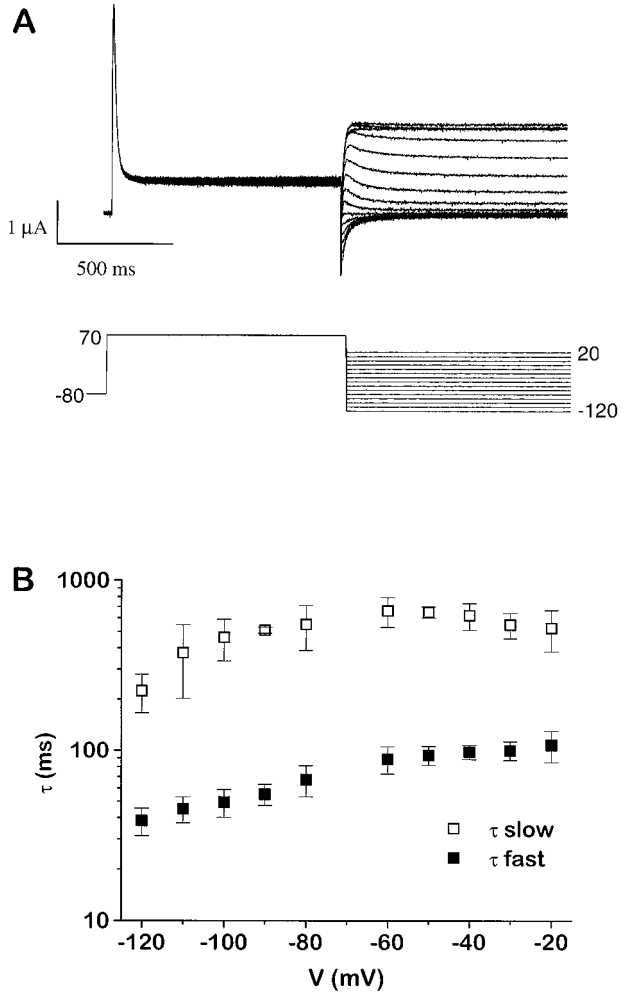

Figure 6. Deactivation kinetics in Melk2 channels. *A*, Deactivation kinetics were determined by first activating (and inactivating) channels with a 1 sec pulse to 70 mV. This was followed by a series of 3 sec pulses from 20 to −120 mV, during which currents initially increased in amplitude as a result of recovery from inactivation, followed by current decay attributable to channel closure. These decaying currents were best fit with the sum of two exponentials as in Figure 4*A*, and time constants derived from these fits (τ_{fast} and τ_{slow}) are plotted in *B* and listed in Table 2. Calibration: 1 μA, 1 sec. *Points* in *B* are mean ± SD; $n = 10$ for each point.

Table 2. Deactivation time constants as in Figure 6

	Deactivation τ (msec)	
V_m (mV)	Fast	Slow
−120	38.5 ± 7.0	223 ± 57
−110	45.2 ± 7.7	374 ± 172
−100	49.6 ± 9.3	461 ± 127
−90	55.3 ± 7.9	509 ± 21
−80	67.3 ± 13.9	551 ± 163
−70	ND	ND
−60	89.0 ± 16.1	652 ± 49
−50	93.7 ± 11.8	622 ± 110
−40	98.1 ± 9.4	549 ± 93
−30	99.6 ± 12.5	524 ± 143
−20	107.7 ± 22.6	380 ± 127

Values are mean ± SD; $n = 4$, ND, Not determined.

The Melk2 steady-state inactivation relation was determined using the voltage protocol shown in Figure 8*B*, based on a similar protocol used to measure steady-state inactivation in HERG channels (Smith et al., 1996). A 1 sec pulse to 70 mV was used to maximally activate and then inactivate channels. Conditioning pulses of 40 msec ranging from 70 to −100 mV were subsequently presented to allow channels to equilibrate between inactivated and open states (see Fig. 8 legend for the correction procedure for channels entering the closed state at more negative voltages). The proportion of channels available to conduct at the end of each conditioning pulse was determined by measuring the instantaneous current values by a subsequent step back to 70 mV, as indicated by Figure 8*B, large arrow*. These values were normalized to the maximum instantaneous current value obtained and plotted as a conductance (g/g_{max}) versus voltage (Fig. 8*C, filled circles*). The resulting curve represents the steady-state inactivation relation, which when fit with a Boltzmann function has a $V_{½}$ of −2.45 ± 1.01 mV and a slope factor of 21.54 ± 1.01 mV per e-fold change in conductance ($n = 3$).

The nonlinear *I–V* relation shown in Figure 3*B* should be predicted by the steady-state activation and inactivation relations if we have correctly identified and characterized the predominant gating processes. To test this, we multiplied the steady-state activation and inactivation relations. Their product yields a bell-shaped steady-state conductance–voltage curve (Fig. 8*C, open symbols*). An *I–V* relationship calculated from this steady-state conductance–voltage relation closely matches the experimental *I–V* relationship determined at 1 sec (Fig. 8*D*; data from Fig. 3*B*). This agreement between the predicted and observed results suggests that inactivation causes rectification of the Melk *I–V* relationship, as in HERG channels (Smith et al., 1996), and that we have accounted for the primary determinants of the steady-state Melk2 currents in our analysis.

C-type inactivation in Melk channels

Rapid inactivation causing inward rectification in HERG channels is attributable to a C-type inactivation mechanism (Schonherr and Heinemann, 1996; Smith et al., 1996; Herzberg et al., 1998). To test the possibility that a similar mechanism was responsible for the inactivation seen in Melk2, we first determined whether external TEA^+ slows inactivation as it does for Shaker (Choi et al., 1991;) and HERG channels (Smith et al., 1996). We found that TEA^+ slows inactivation (Fig. 9*A*), with a $K_{½}$ of 97 ± 16 mM, as determined from a plot of inactivation rate ($1/\tau$) versus log [TEA^+] (Fig. 9*B*). Although the sensitivity to TEA^+ is less for Melk2 currents than for Shaker ($K_{½}$ = 33 mM; Choi et al., 1991) or HERG ($K_{½}$ = 20 mM; Smith et al., 1996), this result supports the hypothesis of a C-type inactivation mechanism in Melk.

As a second test of this hypothesis we determined the effects of two point mutations in the P region predicted to impair C-type inactivation. One of these mutations, S475A, is at a site equivalent to a residue involved in C-type inactivation in Shaker (Lopez-Barneo et al., 1993) and in HERG (Schonherr and Heinemann 1996; Smith et al., 1996; Ficker et al., 1998; Herzberg et al., 1998; Fig. 1, *asterisk*). The second mutation, S464T, is equivalent to a mutation in HERG channels that eliminates C-type inactivation (Suessbrich et al., 1997; Ficker et al., 1988; Herzberg et al., 1998). To characterize inactivation in these channels, the current measured at the end of the voltage pulse ($I_{1\ sec}$) was

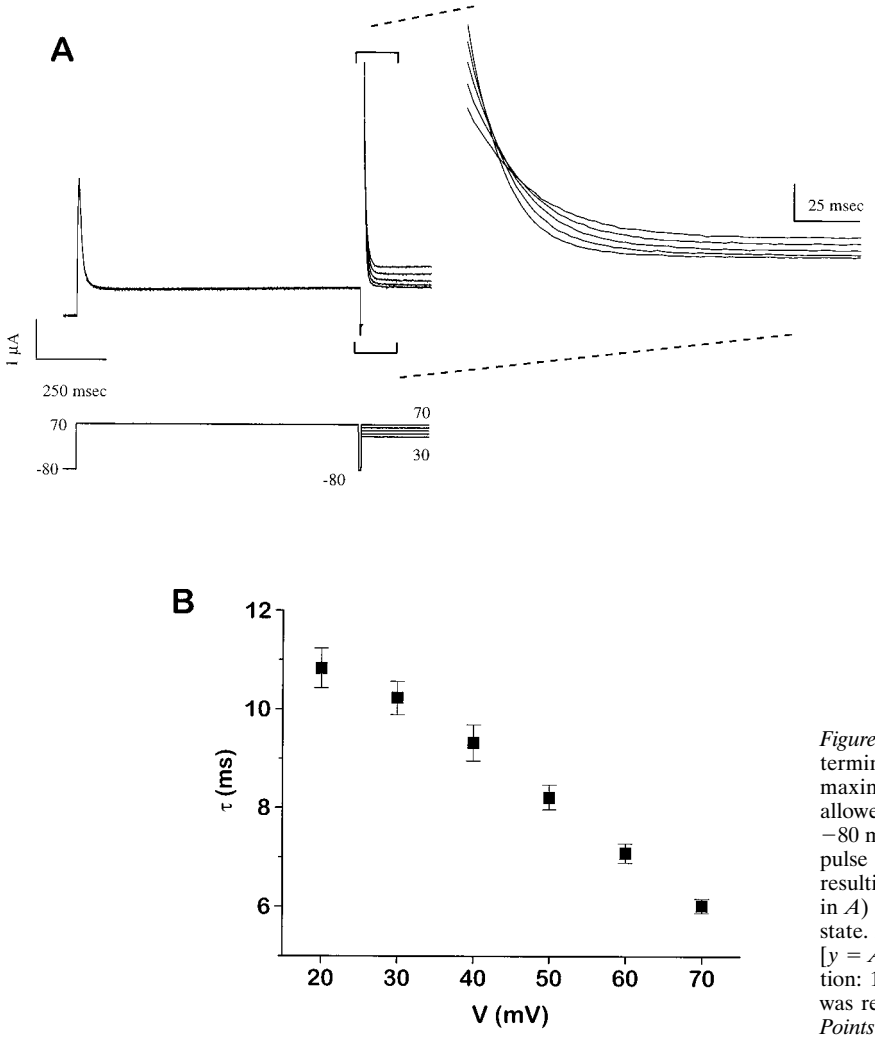

Figure 7. Melk2 inactivation kinetics. *A*, Inactivation was determined with a three-pulse voltage paradigm. Channels were maximally inactivated by a 1 sec pulse to 70 mV and then allowed to recover from inactivation with a 10 msec pulse to −80 mV. Before substantial channel deactivation a subsequent pulse to a voltage ranging from 70 to 20 mV was given. The resulting inactivating currents in *A* (and in the expanded view in *A*) represent channels going from the open to the inactive state. *B*, Time constants derived from a single exponential fit [$y = Ae^{-(t/\tau)}$] to these currents are shown in Table 3. Calibration: 1 μA, 250 msec. A 1 msec duration capacitance artifact was removed before the inactivating currents in *A* for clarity. *Points* in *B* are mean ± SD.

Table 3. Inactivation time constants as in Figure 7

V_m (mV)	Inactivation τ (msec)
20	10.8 ± 1.15
30	10.2 ± 1.24
40	9.3 ± 1.10
50	8.2 ± 0.84
60	7.1 ± 0.71
70	6.0 ± 0.68

Values are mean ± SD; $n = 4$.

normalized to the instantaneous peak current in the absence of inactivation determined from the three-pulse protocol (I_{max}) and plotted as a function of voltage in each case (Fig. 10*A–D*). The relative inactivation rates of the mutants were obtained from the relaxation from I_{max}, which is replotted on a faster time scale in Figure 10*E*. Compared with wild-type channels, the S475A mutation produces less inward rectification and slower inactivation, whereas S464T eliminates rectification as well as inactivation. These effects parallel those of the equivalent mutations in HERG channels (Suessbrich et al., 1997; Ficker et al., 1998; Herzberg et al., 1998) and in Shaker channels (Lopez-Barneo et al., 1993), providing further support for the hypothesis that a C-type inactivation mechanism is responsible for the inactivation of Melk2 channels.

Table 4. Recovery from activation

V_m (mV)	Recovery from Inactivation τ (msec)
−80	3.1 ± 0.2
−70	3.6 ± 0.7
−60	4.9 ± 1.0
−50	6.7 ± 1.0
−40	6.8 ± 0.8
−30	8.5 ± 1.3
−20	10.8 ± 1.3
−10	12.6 ± 1.2
0	14.5 ± 1.3
10	16.0 ± 1.2
20	16.5 ± 1.1

Values are mean ± SD; $n = 8$.

Comparison of currents from Eag family members

To further distinguish Melk2 channels from other members of the Eag family, we compared the rectification and underlying inactivation properties of Meag, HERG, and Melk, representatives of each Eag subfamily (Fig. 11). Scaling the currents evoked by the three-pulse protocol (as described for Fig. 10) to the maximum instantaneous current obtained during the third pulse

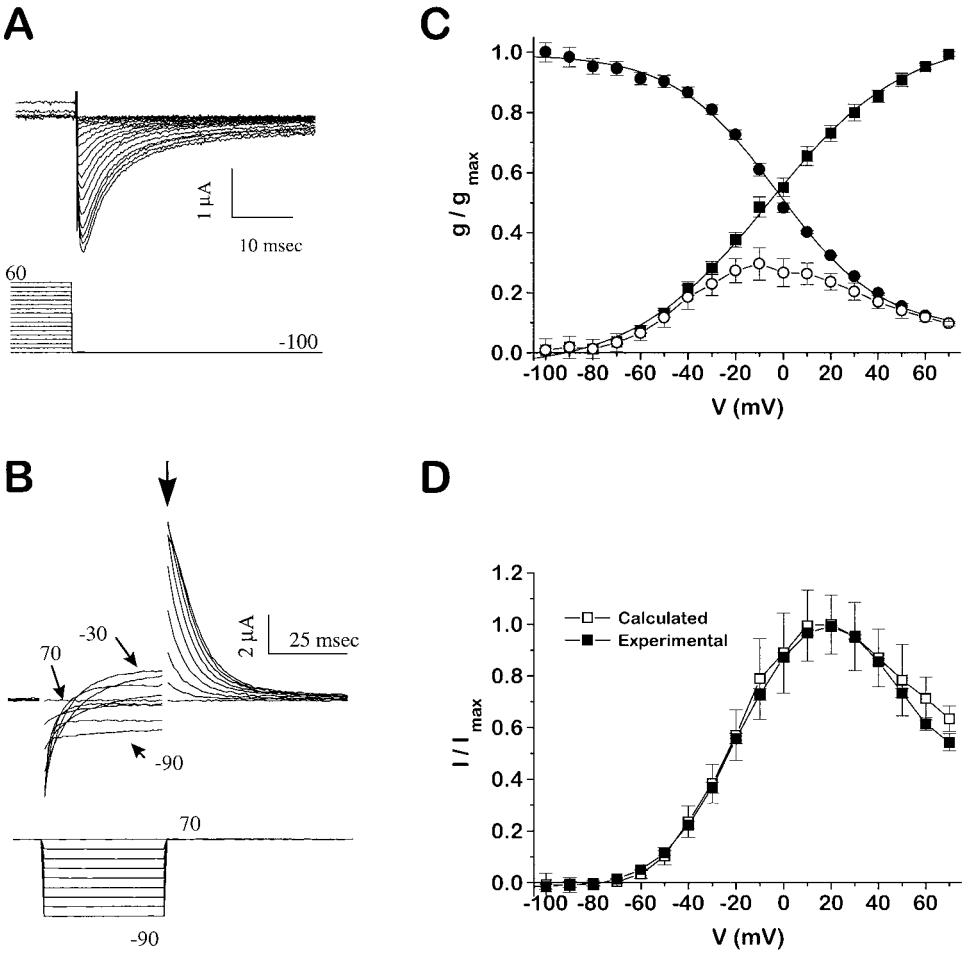

Figure 8. Steady-state properties. *A*, Tail current protocol used to generate steady-state activation curve. Inward tail currents were elicited at −100 mV after 3 sec voltage commands from −100 to 70 mV from rest at −80 mV. Only the last 10 msec of the 3 sec pulses are shown. The decay phase was fit with the sum of two exponentials [$y = A_{fast}e^{-(t/\tau fast)} + A_{slow}e^{-(t/\tau slow)}$] and extrapolated to the onset of the −100 mV pulse to minimize the effects of recovery from inactivation (the rising phase of the tail current). *B*, Protocol for generating steady-state inactivation curve. Channels were first activated (and then inactivated) by a 1 sec pulse to 70 mV (only 10 msec of which is shown in *B*) and then were allowed to equilibrate between open and inactive states during a conditioning pulse ranging from 70 to −100 mV. A second pulse to 70 mV was then given to determine the proportion of channels in the open state from the instantaneous current thus evoked. *C*, Steady-state activation curve (*filled squares*) generated from values from *A* normalized to the largest value, plotted versus command voltage and fit with a single power Boltzmann function of the form $y = 1 - \{1/[1 + e^{(V - V_{½})/k}]\}$. The half-maximal voltage of activation ($V_{½}$) is −6.37 ± 1.43 mV per e-fold change in conductance with a slope factor (k) of 28.43 ± 1.55 mV; $n = 8$. The steady-state inactivation curve (*filled circles*) was generated from normalized instantaneous current values from *B* plotted as a conductance versus the conditioning voltage and fit with a single power Boltzmann function of the form $y = 1/[1 + e^{(V - V_{½})/k}]$, resulting in a $V_{½}$ of −2.45 ± 1.01 mV and $k = 21.54 \pm 1.01$ mV; $n = 3$. Channel deactivation also affects the peak taken at the *arrow*, especially during negative conditioning pulses from −100 to approximately −50 mV. This was corrected for by estimating the relative amount of closure during the 40 msec conditioning pulse based on the deactivation time constant, where % deactivation = $1 - (1/e)(40 \text{ msec}/\tau_{\text{fast deactivation}})$ ($\%A\tau_{\text{fast deactivation}}$) and adding this correction to the availability curve. A 1 msec capacitance artifact was removed at the beginning and end of the conditioning pulse. *Open circles* represent steady-state conductance calculated by multiplying the activation and inactivation curves on the same plot. The error in the calculated conductance is the sum of the errors in the steady-state curves. *D*, The calculated *I–V* relation (*open symbols*) was determined from the conductance in *C*, adjusted for the effects of driving force in accord with Ohm's law, where $I_{\text{calculated}} = (g_{\text{calculated}})(V_m - E_{rev})$, and scaled to the largest value (V_m = membrane potential, and E_{rev} = reversal potential). The experimental *I–V* relation is the same as that from Figure 3*B*, except that it is scaled to its largest value at the end of the voltage pulse, instead of the beginning of the pulse, for comparison of nonlinearity.

(I_{max}) provides a visual impression of the differences in rectification among the three channel types (compare the current amplitudes at $I_{1\ sec}$ and I_{max}; Fig. 11*A–C*). Comparison of the steady-state *I–V* relations reflects these differences and shows that Melk is intermediate to Meag, which has little or no inward rectification, and HERG, which is strongly rectifying (Fig. 11*D*). Correspondingly, the inactivation rate of Melk2 is intermediate to that of Meag, which is noninactivating, and HERG, which inactivates rapidly (Fig. 11*E*). Thus, the rate and extent of C-type inactivation is a distinguishing feature for different subfamilies of potassium channels within the Eag family.

Sensitivity to E-4031

A defining characteristic of channels in the Erg subfamily is a nanomolar sensitivity to class III antiarrhythmic drugs such as dofetilide and E-4031 (Trudeau et al., 1995; Snyders and Chaudhary, 1996; Spector et al., 1996a; London et al., 1997; Shi et al., 1997; Zhou et al., 1998). In contrast, Meag (Herzberg et al., 1998) and bovine Eag (Ficker et al., 1998) channels have 100-fold less sensitivity to these drugs. We determined the effects of E-4031 on Melk channels and found that Melk currents elicited by a pulse to 20 mV after equilibration at −5 mV in 5 μM E-4031 for 10 min were no different from currents in the absence of drug (data not shown). This is a somewhat surprising result, because HERG and Melk channels share all the residues in the P loop that have previously been identified as determinants of drug binding in HERG (Ficker et al., 1998).

Physiological roles of Melk2 channels

To begin to address the physiological roles played by Melk2 channels in the brain, we presented a ramp voltage-clamp command to 60 mV with a rise time of 3 msec and repolarizing ramps of varying durations (Fig. 12). A sharp peak of outward current is evoked by the initial depolarizing ramp as channels activate and subsequently inactivate, indicating that Melk2 could potentially contribute to the repolarization of a single action potential. As the duration of the repolarizing ramp increases, a second peak of current emerges as a result of the recovery from inactivation, suggesting that during a long burst of action potentials Melk2 currents might contribute to the timing of burst duration or to

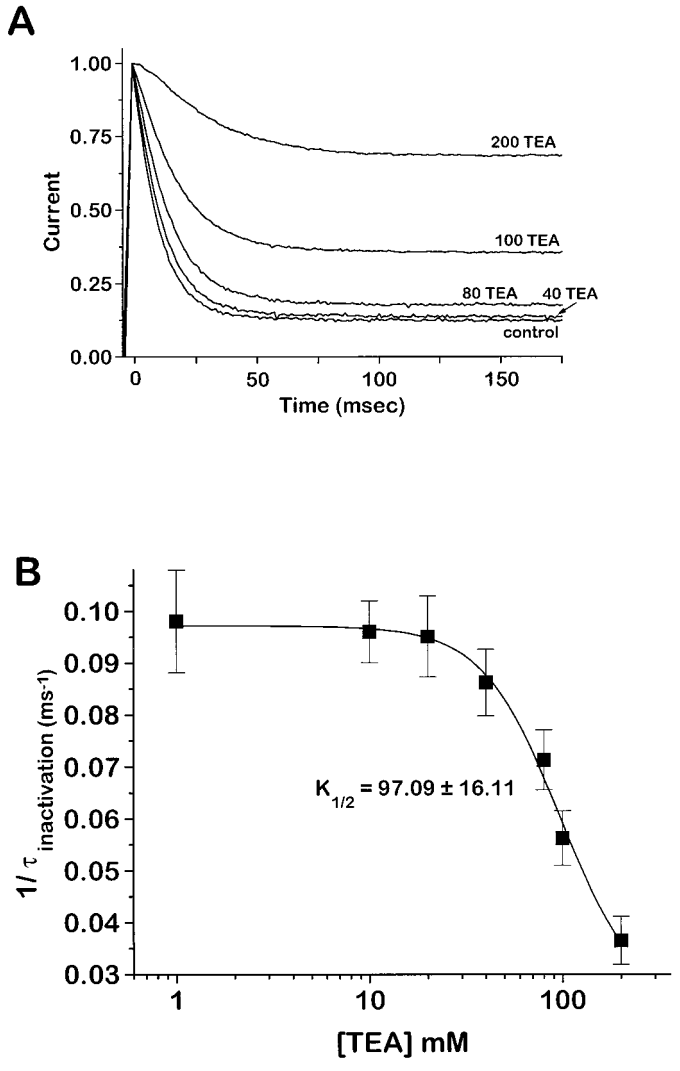

Figure 9. TEA slows Melk2 inactivation. *A*, Inactivating currents after a second step to 70 mV (as in Fig. 7*A*) in the presence of increasing amounts of external TEA^+ as indicated. Currents were normalized to their peaks to better compare the effects of TEA^+. The *bottom axis* represents the time after the second pulse to 70 mV. *B*, The inverse of the time constant of inactivation ($1/\tau$) plotted versus [TEA^+] was fit with a sigmoidal function of the form $y = 1/[1 + [TEA^+]/K_{½})]$, which yields a half-maximal concentration ($K_{½}$) for slowing inactivation of 97.09 ± 16.11 mM TEA^+; $n = 3$ for 200 mM TEA^+; $n = 6$ for all other concentrations of TEA^+ (mean ± SD).

spike frequency adaptation. Thus, their particular gating properties render Melk2 channels well suited to a dual role in membrane excitability—on a short (millisecond) time scale to the control of membrane potential and on a longer (hundreds of milliseconds) time scale to the regulation of firing frequency or burst duration.

DISCUSSION

The novel properties of Melk2 channels described in this study expand our understanding of the structural and functional diversity within the Eag family and provide physiological and pharmacological criteria with which the corresponding currents *in vivo* may be distinguished. *Melk2* mRNA is highly expressed in brain tissue and not in heart, spleen, lung, liver, skeletal muscle, or kidney; a smaller band appears in testis, but it is not yet clear whether this represents a true *Melk2* transcript. In contrast, members of the Erg family are broadly distributed in tissues such as the brain, heart, skeletal muscle, smooth muscle, and testis (Curran et al., 1995; London et al., 1997; Shi et al., 1997; Wymore et al., 1997), and Eag members are found in the brain, skeletal muscle, and the retina (Ludwig et al., 1994; Frings et al., 1998).

A distinctive feature of Melk2 currents is a large, early inactivating component and a corresponding inward rectification that is intermediate in degree to the strongly rectifying HERG and the noninactivating Meag. Inactivation occurs by a voltage-dependent, C-type inactivation mechanism such as that mediating inward rectification in HERG channels. Melk2 currents lack the Cole–Moore shift and sensitivity of activation kinetics to Mg^{2+} observed in Eag subfamily members as well as the E-4031 sensitivity characteristic of HERG.

The inactivation mechanism in Melk2 appears to be highly conserved with the C-type inactivation mechanism described for HERG channels. For example, the mutation S464T in Melk essentially removes inactivation, as does the equivalent mutation S620T in HERG, whereas Melk2 S475A slows inactivation like S631A in HERG (Suessbrich et al., 1997; Herzberg et al., 1998). This suggests a similar dependence on the side chains of the amino acid residues present at these two sites in the P region for control of inactivation in Melk2 and HERG channels. The essentially null inactivation phenotype of Melk2 S464T also suggests that additional mechanisms such as N-type inactivation do not contribute to the inactivation of Melk2 channels.

Despite these similarities, Melk2 inactivation is approximately threefold to fourfold slower, and the $V_{½}$ of the steady-state inactivation relation is shifted by ~80 mV compared with the corresponding properties of HERG (cf. Smith et al., 1996). These differences may arise from other residues involved in C-type inactivation that are not conserved between Melk2 and HERG. For example, the rate of C-type inactivation appears to be proportional to the volume of the amino acid side chain at equivalent sites in S6 in ShakerB (463; Hoshi et al., 1991) and HERG (644; Herzberg et al., 1998). In each case an alanine, with the smaller volume, is associated with slow inactivation, whereas when the larger valine is present, inactivation is fast. In Melk2 channels the inactivation rate is intermediate, as predicted by the intermediate volume of the threonine at the corresponding position (T488) and consistent with the hypothesis that this site may contribute to the differences in C-type inactivation between HERG and Melk2 channels.

Melk2 activation properties are distinct from those in either the Eag or Erg channel subfamilies. Macroscopic Melk2 activation is well described by the sum of two exponentials with time constants similar to those of rat Eag channels (Terlau et al., 1996); the $V_{½}$ and the slope of Melk2 g–V relation are similar to those of Meag channels (Robertson et al., 1996). These properties distinguish Melk2 from HERG, which has very slow and sigmoidal activation kinetics and a g–V relation that is twofold to threefold steeper and shifted by approximately −25 mV (Sanguinetti et al., 1995; Trudeau et al., 1995; Wang et al., 1997). However, unlike Eag, but similar to HERG, Melk2 activation does not exhibit a Cole–Moore shift, which is attributed to residency in a remote closed state during a hyperpolarizing prepulse; during a subsequent depolarization, the transition from that closed state is rate limiting (Young and Moore 1981; Bezanilla et al., 1994). Melk2 channels correspondingly lack a sensitivity to external divalent cations, which, like hyperpolarizing prepulses, slow activation in Eag channels (Terlau et al., 1996). This property has recently been used as a criterion to link Eag-type channels with I_{Kx}, a

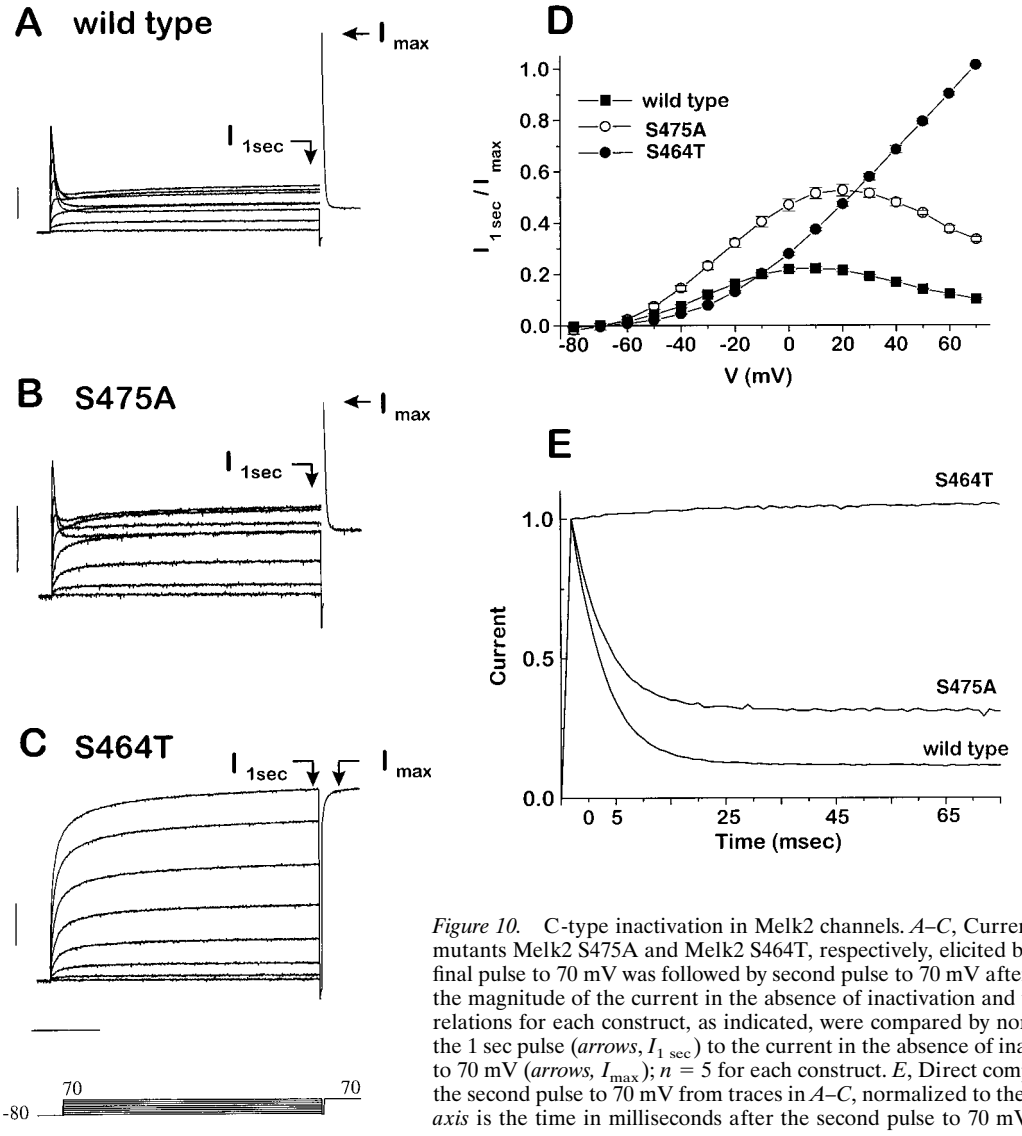

Figure 10. C-type inactivation in Melk2 channels. *A–C*, Current families of wild-type Melk2 and point mutants Melk2 S475A and Melk2 S464T, respectively, elicited by voltage steps from −70 to 70 mV. The final pulse to 70 mV was followed by second pulse to 70 mV after a 10 msec pulse to −80 mV to estimate the magnitude of the current in the absence of inactivation and the inactivation rate. *D*, Normalized *I–V* relations for each construct, as indicated, were compared by normalizing the current level at the end of the 1 sec pulse (*arrows*, $I_{1\ sec}$) to the current in the absence of inactivation at the peak of the second pulse to 70 mV (*arrows*, I_{max}); $n = 5$ for each construct. *E*, Direct comparison of the inactivating currents from the second pulse to 70 mV from traces in *A–C*, normalized to the peak current for each trace. The *bottom axis* is the time in milliseconds after the second pulse to 70 mV. Calibration: *A–C*, 1 μA, 250 msec.

current involved in sensory transduction in the retina (Frings et al., 1998). It is interesting that the voltage dependence of activation in Melk2 is similar to that of Meag despite the presence of a proline residue in S4 (P347) instead of the conserved arginine residue present in Eag and HERG channels. Whether the presence or absence of this charged residue in S4 contributes to differences in voltage sensitivity among the Eag family members remains to be determined.

Melk deactivation gating is similar to that of certain isoforms of Merg1 channels that have shortened or novel N-terminal domains (Lees-Miller et al., 1997; London et al., 1997) and HERG channels with engineered deletions of the N terminus (Schonherr and Heinemann 1996; Spector et al., 1996b; Wang et al., 1998). In wild-type HERG and Merg1a channels (both of which have long N termini) the N terminus modulates deactivation kinetics, but in the absence of this domain, deactivation kinetics are ~100-fold faster. The S4–S5 linker is also critically involved in this process and may form a receptor site for the interaction of the N terminus with the pore region (Wang et al., 1998). The relatively rapid deactivation kinetics in Melk2 channels suggest that such modulation may not occur in these channels; perhaps the shorter N terminus of Melk2 or amino acid differences in the S4–S5 linker fail to support the modulatory mechanism. Further experiments will be required to test these hypotheses.

One of the hallmark features of the Erg family of channels is their sensitivity to inhibition by class III antiarrhythmic drugs (Trudeau et al., 1995; Snyders and Chaudhary 1996; Spector et al., 1996a; London et al., 1997; Shi et al., 1997; Zhou et al., 1998). Efforts at localizing drug binding sites reveal residues in the P loop and part of the S6 domain of HERG necessary for drug block, including S620 and S631 (Ficker et al., 1998). It is interesting that, despite the presence of identical residues at the equivalent positions (S464 and S475 respectively), Melk channels are insensitive to E-4031. Thus other, as yet unidentified residues must also be involved in drug binding in HERG, or alternatively, other Melk residues may disrupt the ability of drug to bind these channels.

A recent report of the cloning and expression of *elk1* from rat (*Relk1*; Shi et al., 1998) reveals heterogeneity within the Elk subfamily. In contrast to *Melk2*, which is expressed robustly in brain, mRNA levels of *Relk1* were barely detectable in brain but were much higher in sympathetic ganglia and sciatic nerve (Shi et al., 1998). The amino acid sequences of the corresponding polypeptides are ~68% identical and form channels with distinct

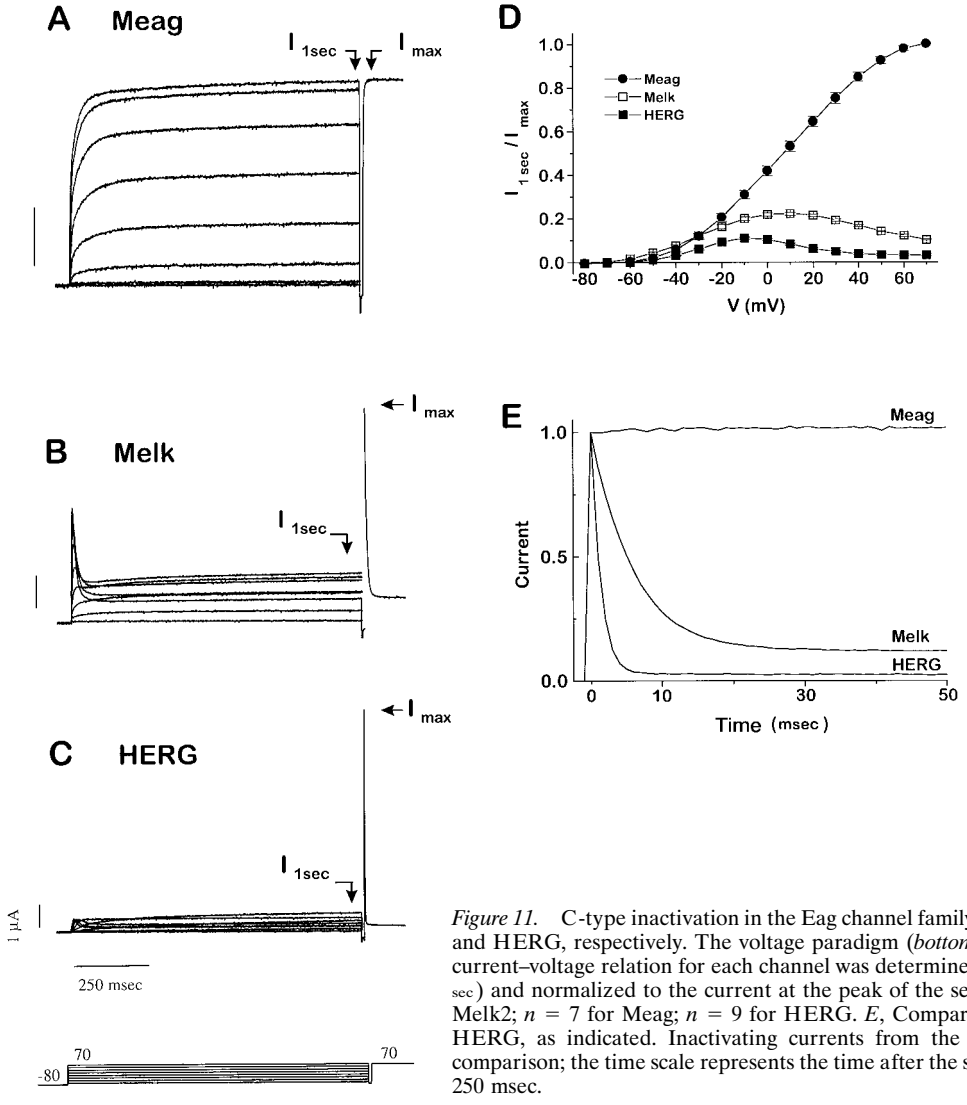

Figure 11. C-type inactivation in the Eag channel family. *A–C*, Families of currents from Meag, Melk2, and HERG, respectively. The voltage paradigm (*bottom*) is identical to the one in Figure 10. *D*, The current–voltage relation for each channel was determined at the end of a 1 sec voltage pulse (*arrows*, $I_{1\,sec}$) and normalized to the current at the peak of the second pulse to 70 mV (*arrows,* I_{max}); $n = 5$ for Melk2; $n = 7$ for Meag; $n = 9$ for HERG. *E*, Comparison of inactivation among Meag, Melk2, and HERG, as indicated. Inactivating currents from the second pulse to 70 mV are normalized for comparison; the time scale represents the time after the second pulse to 70 mV. Calibration: *A–C*, 1 μA, 250 msec.

biophysical properties. For example, Melk2 exhibits relatively rapid activation and inactivation, whereas Relk1 is slow to activate and shows no apparent inactivation (cf. Shi et al., 1998).

The pronounced differences in gating among channels in the Eag family likely reflect their distinct physiological roles. HERG currents peak not during activation but rather as channels recover from inactivation before returning to the closed or resting state (Sanguinetti et al., 1995; Trudeau et al., 1995). Thus, HERG is specialized to contribute a large repolarizing current at the terminal repolarization phase of the cardiac action potential (Zhou et al., 1998), as previously demonstrated for the native I_{Kr} (Zeng et al., 1995). In contrast, the faster activation and slower inactivation of Melk2 channels gives rise to early transient peaks, which occur on a time scale that may enable them to contribute a repolarizing current during a neuronal action potential or short spike train. Like HERG, however, Melk2 recovers from inactivation more rapidly than it deactivates and thus may contribute a second outward, repolarizing current near the end of a sustained burst, especially in conjunction with other K^+ currents that initiate the repolarization process. In neurons with action potentials that have late plateau phases (cf. McCormick et al., 1997), this second outward component could be a significant factor in neuronal processing.

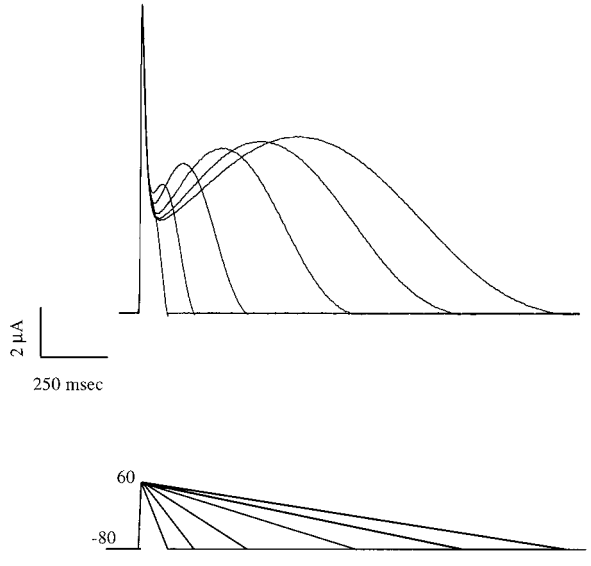

Figure 12. Melk2 currents in response to voltage ramps. Voltage was changed from rest (−80 mV) to 60 mV with a 3 msec ramp for all traces and then returned to rest with a ramp of the following durations: 100, 200, 400, 800, 1200, and 1600 msec. The same results were obtained in three additional experiments. Calibration: 2 μA, 250 msec.

REFERENCES

Barish ME (1983) A transient calcium-dependent chloride current in the immature *Xenopus* oocyte. J Physiol (Lond) 342:309–325.

Bezanilla F, Perozo E, Stefani E (1994) Gating of Shaker K^+ channels: II. The components of gating currents and a model of channel activation. Biophys J 66:1011–1021.

Choi KL, Aldrich RW, Yellen G (1991) Tetraethylammonium blockade distinguishes two inactivation mechanisms in voltage-activated K^+ channels. Proc Natl Acad Sci USA 88:5092–5095.

Cole KS, Moore JW (1960) Ionic current measurements in the squid giant axon membrane. J Gen Physiol 44:123–167.

Curran ME, Splawski I, Timothy KW, Vincent GM, Green ED, Keating MT (1995) A molecular basis for cardiac arrhythmia: HERG mutations cause long QT syndrome. Cell 80:795–803.

Drysdale R, Warmke J, Kreber R, Ganetzky B (1991) Molecular characterization of *eag*: a gene affecting potassium channels in *Drosophila melanogaster*. Genetics 127:497–505.

Ficker E, Jarolimek W, Kiehn J, Baumann A, Brown AM (1998) Molecular determinants of dofetilide block of HERG K^+ channels. Circ Res 82:386–395.

Frings S, Brull N, Dzeja C, Angele A, Hagen V, Kaupp UB, Baumann A (1998) Characterization of ether-à-go-go channels present in photoreceptors reveals similarity to I_{K_x}, a K^+ current in rod inner segments. J Gen Physiol 111:583–599.

Ganetzky B, Wu CF (1983) Neurogenetic analysis of potassium currents in *Drosophila*: synergistic effects on neuromuscular transmission in double mutants. J Neurogenet 1:17–28.

Herzberg IM, Trudeau MC, Robertson GA (1998) Transfer of rapid inactivation and E-4031 sensitivity from HERG to M-EAG channels. J Physiol (Lond) 511:3–14.

Higuchi R (1990) PCR protocols: a guide to methods and applications (Innis MA, Gelfand DH, Sninsky JJ, White TJ, eds), pp 177–183. New York: Academic.

Hoshi T, Zagotta WN, Aldrich RW (1991) Two types of inactivation in Shaker K^+ channels: effects of alterations in the carboxy-terminal region. Neuron 7:547–556.

Lees-Miller JP, Kondo C, Wang L, Duff HJ (1997) Electrophysiological characterization of an alternatively processed ERG K^+ channel in mouse and human hearts. Circ Res 81:719–726.

Liman ER, Tytgat J, Hess P (1992) Subunit stoichiometry of a mammalian K^+ channel determined by construction of multimeric cDNAs. Neuron 9:861–871.

London B, Trudeau MC, Newton KP, Beyer AK, Copeland NG, Gilbert DJ, Jenkins NA, Satler CA, Robertson GA (1997) Two isoforms of the mouse ether-a-go-go-related gene coassemble to form channels with properties similar to the rapidly activating component of the cardiac delayed rectifier K^+ current. Circ Res 81:870–878.

Lopez-Barneo J, Hoshi T, Heinemann SH, Aldrich RW (1993) Effects of external cations and mutations in the pore region on C-type inactivation of Shaker potassium channels. Receptors Channels 1:61–71.

Ludwig J, Terlau H, Wunder F, Bruggemann A, Pardo LA, Marquardt A, Stuhmer W, Pongs O (1994) Functional expression of a rat homologue of the voltage gated either a go-go potassium channel reveals differences in selectivity and activation kinetics between the *Drosophila* channel and its mammalian counterpart. EMBO J 13:4451–4458.

McCormick DA, Bal T (1997) Sleep and arousal: thalamocortical mechanisms. Annu Rev Neurosci 20:185–215.

Pajor AM, Wright EM (1992) Cloning and functional expression of a mammalian Na^+/nucleoside cotransporter. A member of the SGLT family. J Biol Chem 267:3557–3560.

Robertson GA, Warmke JM, Ganetzky B (1996) Potassium currents expressed from *Drosophila* and mouse eag cDNAs in *Xenopus* oocytes. Neuropharmacology 35:841–850.

Sanguinetti MC, Jurkiewicz NK (1990) Two components of cardiac delayed rectifier K^+ current. Differential sensitivity to block by class III antiarrhythmic agents. J Gen Physiol 96:195–215.

Sanguinetti MC, Jiang C, Curran ME, Keating MT (1995) A mechanistic link between an inherited and an acquired cardiac arrhythmia: HERG encodes the I_{Kr} potassium channel. Cell 81:299–307.

Schonherr R, Heinemann SH (1996) Molecular determinants for activation and inactivation of HERG, a human inward rectifier potassium channel. J Physiol (Lond) 493:635–642.

Shi W, Wymore RS, Wang HS, Pan Z, Cohen IS, McKinnon D, Dixon JE (1997) Identification of two nervous system-specific members of the erg potassium channel gene family. J Neurosci 17:9423–9432.

Shi W, Wang HS, Pan Z, Wymore RS, Cohen IS, McKinnon D, Dixon JE (1998) Cloning of a mammalian elk potassium channel gene and EAG mRNA distribution in rat sympathetic ganglia. J Physiol (Lond) 511:675–682.

Shibasaki T (1987) Conductance and kinetics of delayed rectifier potassium channels in nodal cells of the rabbit heart. J Physiol (Lond) 387:227–250.

Smith PL, Baukrowitz T, Yellen G (1996) The inward rectification mechanism of the HERG cardiac potassium channel [see comments]. Nature 379:833–836.

Snyders DJ, Chaudhary A (1996) High affinity open channel block by dofetilide of HERG expressed in a human cell line. Mol Pharmacol 49:949–955.

Spector PS, Curran ME, Keating MT, Sanguinetti MC (1996a) Class III antiarrhythmic drugs block HERG, a human cardiac delayed rectifier K^+ channel. Open-channel block by methanesulfonanilides. Circ Res 78:499–503.

Spector PS, Curran ME, Zou A, Keating MT, Sanguinetti MC (1996b) Fast inactivation causes rectification of the I_{Kr} channel. J Gen Physiol 107:611–619.

Suessbrich H, Schonherr R, Heinemann SH, Lang F, Busch AE (1997) Specific block of cloned Herg channels by clofilium and its tertiary analog LY97241. FEBS Lett 414:435–438.

Terlau H, Ludwig J, Steffan R, Pongs O, Stuhmer W, Heinemann SH (1996) Extracellular Mg^{2+} regulates activation of rat eag potassium channel. Pflugers Arch 432:301–312.

Trudeau MC, Warmke JW, Ganetzky B, Robertson GA (1995) HERG, a human inward rectifier in the voltage-gated potassium channel family. Science 269:92–95.

Trudeau MC, Warmke JW, Ganetzky B, Robertson GA (1996) HERG sequence correction [letter]. Science 272:1087.

Wang J, Trudeau MC, Zappia AM, Robertson GA (1998) Regulation of deactivation by an amino terminal domain in HERG potassium channels. J Gen Physiol 112:637–647.

Wang S, Morales MJ, Liu S, Strauss HC, Rasmusson RL (1996) Time, voltage and ionic concentration dependence of rectification of h-erg expressed in *Xenoaus* oocytes. FEBS Lett 389:167–173.

Wang S, Liu S, Morales MJ, Strauss HC, Rasmusson RL (1997) A quantitative analysis of the activation and inactivation kinetics of HERG expressed in *Xenopus* oocytes. J Physiol (Lond) 502:45–60.

Warmke JW, Ganetzky B (1994) A family of potassium channel genes related to eag in *Drosophila* and mammals. Proc Natl Acad Sci USA 91:3438–3442.

Warmke J, Drysdale R, Ganetzky B (1991) A distinct potassium channel polypeptide encoded by the *Drosophila* eag locus. Science 252:1560–1562.

Wu CF, Ganetzky B, Haugland FN, Liu AX (1983) Potassium currents in *Drosophila*: different components affected by mutations of two genes. Science 220:1076–1078.

Wymore RS, Gintant GA, Wymore RT, Dixon JE, McKinnon D, Cohen IS (1997) Tissue and species distribution of mRNA for the I_{Kr}-like K^+ channel, erg. Circ Res 80:261–268.

Young SH, Moore JW (1981) Potassium ion currents in the crayfish giant axon. Dynamic characteristics. Biophys J 36:723–733.

Zeng J, Laurita KR, Rosenbaum DS, Rudy Y (1995) Two components of the delayed rectifier K^+ current in ventricular myocytes of the guinea pig type. Theoretical formulation and their role in repolarization. Circ Res 77:140–152.

Zhou Z, Gong Q, Ye B, Fan Z, Makielski JC, Robertson GA, January CT (1998) Properties of HERG channels stably expressed in HEK 293 cells studied at physiological temperature. Biophys J 74:230–241.